SCIENTIFIC REPORTS

OPEN

Remodeling pathway control of mitochondrial respiratory capacity by temperature in mouse heart: electron flow through the Q-junction in permeabilized fibers

Received: 7 February 2017
Accepted: 18 April 2017
Published online: 06 June 2017

Hélène Lemieux[1,3], Pierre U. Blier[2] & Erich Gnaiger[1]

Fuel substrate supply and oxidative phosphorylation are key determinants of muscle performance. Numerous studies of mammalian mitochondria are carried out (i) with substrate supply that limits electron flow, and (ii) far below physiological temperature. To analyze potentially implicated biases, we studied mitochondrial respiratory control in permeabilized mouse myocardial fibers using high-resolution respirometry. The capacity of oxidative phosphorylation at 37 °C was nearly two-fold higher when fueled by physiological substrate combinations reconstituting tricarboxylic acid cycle function, compared with electron flow measured separately through NADH to Complex I or succinate to Complex II. The relative contribution of the NADH pathway to physiological respiratory capacity increased with a decrease in temperature from 37 to 25 °C. The apparent excess capacity of cytochrome *c* oxidase above physiological pathway capacity increased sharply under hypothermia due to limitation by NADH-linked dehydrogenases. This mechanism of mitochondrial respiratory control in the hypothermic mammalian heart is comparable to the pattern in ectotherm species, pointing towards NADH-linked mt-matrix dehydrogenases and the phosphorylation system rather than electron transfer complexes as the primary drivers of thermal sensitivity at low temperature. Delineating the link between stress and remodeling of oxidative phosphorylation is important for understanding metabolic perturbations in disease evolution and cardiac protection.

Contractile activity in cardiac muscle mainly depends on mitochondrial (mt) energy transformed by oxidative phosphorylation (OXPHOS). The heart is highly sensitive to defects in OXPHOS[1], stress-induced mitochondrial cytopathies and degenerative mitochondrial defects, including heart failure[2,3], acute ischemia and myocardial infarct[4], ischemia-reperfusion[5], type 2 diabetes[6–9], aging[10,11], and inherited genetic diseases[12–15]. Patients present with functional impairment when the capacity of an enzyme is reduced below its threshold activity. This threshold effect is a function of the apparent excess enzyme activity above pathway capacity. To evaluate the threshold and excess capacity of a single step in OXPHOS, it is necessary not only to quantify the changes in enzyme activity, but determine the impact of these changes on respiratory pathway capacity[16].

Respiration in the mammalian heart is supported by carbohydrates (10 to 40%)[17] and fatty acids (60 to 90%)[18]. Electron transfer in the NADH- and succinate-linked pathway (NS-pathway) converges through Complex I and Complex II at the Q-junction[19] (Fig. 1a). Downstream electron flow is catalyzed by Complex III and Complex IV (cytochrome *c* oxidase) to oxygen as the terminal electron acceptor. Conventional protocols in bioenergetics use either NADH-linked substrates (N-pathway) or succinate&rotenone (S-pathway), thereby separating the system into linear thermodynamic cascades, forming distinct electron transfer chains[19–21]. This experimental design aims at the measurement of biochemical coupling efficiency and proton stoichiometry, and is applied in the functional diagnosis of specific OXPHOS defects. As recognized in mitochondrial physiology, however, it

[1]D. Swarovski Research Laboratory, Department of Visceral, Transplant and Thoracic Surgery, Medical University Innsbruck, 6020, Innsbruck, Austria. [2]Laboratoire de Physiologie Animale Intégrative, Université du Québec, Rimouski, QC G5L 3A1, Canada. [3]Present address: Faculty Saint-Jean, University of Alberta, Edmonton, AB T6C 4G9, Canada. Correspondence and requests for materials should be addressed to E.G. (email: erich.gnaiger@oroboros.at)

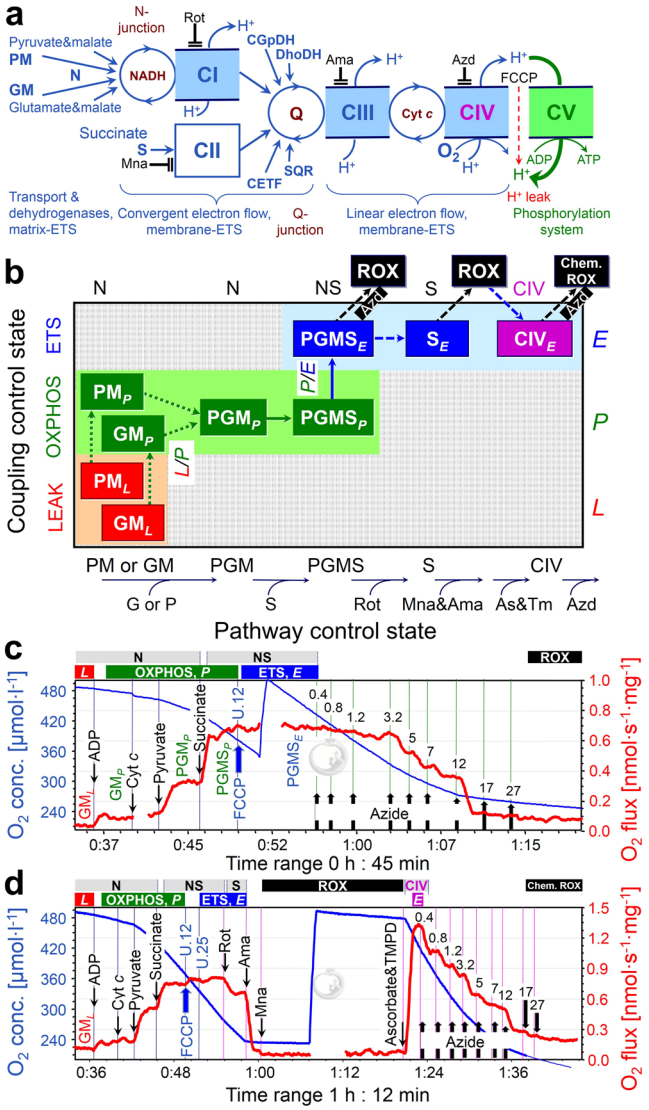

Figure 1. Mitochondrial pathways, substrate-uncoupler-inhibitor-titration (SUIT) protocols and respiration of permeabilized cardiac fibers. (**a**) Schematic representation of the electron transfer system (ETS) coupled to the phosphorylation system (ATP synthase, adenylate translocator and inorganic phosphate transporter). Electron flow from pyruvate&malate (PM) or glutamate&malate (GM) converges at the N-junction (NADH-cycle). Electrons converge at the Q-junction from Complex I (CI, NADH-ubiquinone oxidoreductase), Complex II (CII, succinate-ubiquinone oxidoreductase), glycerophosphate dehydrogenase Complex (CGpDH), electron-transferring flavoprotein Complex (CETF), dihydro-orotate dehydrogenase (DhoDH)[92], sulfide-ubiquinone oxidoreductase (SQR)[93], and choline dehydrogenase (not shown), followed by a linear downstream segment through Complexes III (CIII, ubiquinol-cytochrome *c* oxidoreductase) and CIV (cytochrome *c* oxidase), to the final electron acceptor oxygen. CI, CIII, and CIV are proton pumps generating an electrochemical potential difference across the inner mt-membrane. Coupling of the phosphorylation system with the ETS allows the proton potential to drive phosphorylation of ADP to ATP (coupled flow). Protonophores such as FCCP uncouple the ETS from ATP production. Rotenone, malonate and antimycin A are specific inhibitors of CI, CII and CIII, respectively, and were sequentially added at saturating concentrations. (**b**) Coupling/pathway control diagram illustrating the two protocols starting with either PM or GM (SUIT 1 and 2), convergent electron flow at the Q-junction in the NADH&succinate (NS) pathway, and azide titrations in the NS-pathway control state or single enzyme step of CIV. As&TM, Ascorbate&TMPD. (**c**) SUIT 2a with azide titration in the NS-pathway control state. (**d**) SUIT 2b with azide titration in the CIV single enzyme step as a basis of threshold plots.

does not allow estimation of maximal respiratory capacity under physiological conditions. Fuel substrates supporting convergent electron transfer at the Q-junction enhance respiratory capacity, as shown when succinate is added to NADH-linked substrates, reconstituting physiological tricarboxylic acid cycle function with combined NS-pathway flux. This effect of succinate varies depending on species, strains, organ and experimental conditions; stimulation is 1.6 to 2.0-fold in rat heart[22,23], 1.2 to 1.8-fold in rat skeletal muscle[24–26], 1.4-fold in mouse skeletal muscle[27], and 1.3 to 2.1-fold in human skeletal muscle (reviewed by Gnaiger[28]). Similarly, glycerol-3-phosphate

(Fig. 1a) exerts an additive effect on respiration when combined with pyruvate&malate in rabbit skeletal muscle mitochondria[29], and stimulates respiration beyond NS-pathway capacity in human lymphocytes[30]. Such substrate combinations do not exert completely additive effects on flux due to (i) intersubstrate competition for transport across the inner mt-membrane[31], (ii) regulatory mechanisms in the tricarboxylate acid (TCA) cycle, and (iii) flux control by limiting enzyme capacities downstream of the Q-junction.

With NADH-linked substrates, the major flux control of the N-pathway resides upstream in the dehydrogenases of the TCA cycle, with a high apparent excess capacity of respiratory complexes downstream[16]. Similarly, upstream electron supply limits respiratory capacity in the succinate-pathway. In the physiological state of combined NS-electron supply, flux control is shifted downstream. We therefore examined the apparent excess capacity of cytochrome *c* oxidase (CIV) over convergent NS-pathway flux, and determined the limitation of NS-OXPHOS capacity by the phosphorylation system (Fig. 1a). Mammalian mitochondria are frequently studied at 25 or 30 °C[32]. Temperature coefficients are used to extrapolate the results to 37 °C, but are available for only a few metabolic states[33]. We therefore determined respiration of mouse heart mitochondria in a variety of coupling/pathway control states at 37 °C and different levels of hypothermia[34], i.e. at 30 °C (mild hypothermia), 25 °C (moderate hypothermia) and profound hypothermia (cold storage temperature, 4 °C), and extended our study to hyperthermia (40 °C). Moderate to profound hypothermia reduce myocardial metabolism temporarily and reversibly, and limit ischemic damage during cardiac surgery[35–39], organ preservation[40,41], and preservation of mitochondrial function during preparation of isolated mitochondria and permeabilized fibers[42].

Understanding the control of cell respiration in health and disease requires (i) measurement of mitochondrial pathway control at physiologically and clinically relevant temperatures and (ii) application of substrate combinations which are representative of cellular conditions. These criteria dramatically change our estimation of maximal respiratory capacity and control of mitochondrial respiration, providing a reference for physiological and pharmacological intervention strategies. Our results also provide new perspectives on evolutionary temperature adaptation, suggesting that key control of energy transformation and survival at low temperatures might not primarily be exerted by electron transfer complexes but by (i) upstream elements of the electron transfer system (ETS) including transport of substrates across the inner mitochondrial membrane and matrix dehydrogenases, and (ii) downstream elements of the phosphorylation system.

Results

Pathway control of mitochondrial respiratory capacity. We quantified mitochondrial respiratory capacity in substrate-uncoupler-inhibitor-titration (SUIT) protocols (Figs 1 and 2). Fuel substrates of the N-pathway reduce NAD^+ to NADH at five key steps: pyruvate dehydrogenase, isocitrate dehydrogenase, glutamate dehydrogenase, oxoglutarate dehydrogenase and malate dehydrogenase. Addition of pyruvate (P) to glutamate&malate (GM) increased OXPHOS capacity (PGM_P) by a factor of 2.5 (2.0–3.7) at 37 °C (Fig. 2a,b). In contrast, addition of glutamate (G) to pyruvate&malate (PM) exerted merely a slight stimulatory effect on respiration by a factor of 1.1 (1.0–1.2; Fig. 2b), also observed in rat heart (1.2)[43] and skeletal muscle of the horse (1.2)[44], rabbit (1.2)[29] and humans (1.3)[45]. OXPHOS capacity (ADP-stimulated oxygen flux) was significantly higher with pyruvate&malate compared to glutamate&malate at physiological temperature (PM_P versus GM_P; Fig. 2b). This pattern was reversed at 4 °C, under which conditions N-OXPHOS capacity was higher with GM than PM (Fig. 2c).

In isolated mitochondria or permeabilized fibers incubated with PM, GM or PGM, citrate and 2-oxoglutarate are formed and rapidly exchanged for malate by the tricarboxylate and 2-oxoglutarate carriers, thus limiting the formation of succinate. In addition, succinate is lost into the incubation medium through the active dicarboxylate carrier exchanging succinate for inorganic phosphate. The high malate concentration equilibrates with fumarate, inducing product inhibition of succinate dehydrogenase (CII). Taken together, this limits succinate-linked electron transfer[46]. To simultaneously activate CII and NADH-related dehydrogenases of the TCA cycle, a high exogenous succinate concentration is required in addition to the NADH-linked substrates[47,48], thus simulating the physiological condition of the NS-pathway with convergent electron flow into the Q-junction (Fig. 1a). In the NS-pathway control state (pyruvate&glutamate&malate&succinate; $PGMS_P$, Fig. 1b), respiration almost doubled compared to OXPHOS capacity measured separately through the N- or S-pathway. The respiratory capacity through the S-pathway was similar to that observed with the NADH-linked substrate combinations. This provides evidence for an additive effect of convergent electron flow, expressed in terms of flux control ratios of N/NS = 0.53 (0.40–0.69), and S/NS = 0.61 (0.52–0.82) at 37 °C (Fig. 2b). This additive effect was less pronounced at 4 °C (Fig. 2c), but was similar between 25 °C and 40 °C (Fig. 3).

Temperature sensitivity of respiration depends on metabolic state. We determined temperature coefficients for evaluation of metabolic depression by hypothermia and specific remodeling of pathway control of OXPHOS (Table 1). Mitochondrial content, evaluated by the mitochondrial matrix marker citrate synthase activity, did not differ among tissue preparations. Citrate synthase activity [IU per mg fibers] measured at 30 °C was 0.25 (0.17–0.30), 0.23 (0.16–0.30), 0.24 (0.19–0.26), and 0.22 (0.18–0.28) in the 40, 37, 30 and 25 °C cohort, respectively. Therefore, divergences in mitochondrial content can be ruled out as a confounding factor. NS-OXPHOS capacity declined at 30 and 25 °C by 1.7- and 2.1-fold of the normothermic level (37 °C), and decreased slightly from 37 to 40 °C (Fig. 3; Table 1). The thermal sensitivity of respiration was strongly dependent on coupling/pathway control states (Fig. 4). The Q_{10} is the factor by which the reaction velocity increases for a rise in temperature of 10 °C. It varied between 1.2 and 2.4 across metabolic states in the temperature range of 25 to 37 °C (Fig. 4b; Table 1). The Q_{10} for S-ETS capacity was 1.9 between 30 and 37 °C (Table 1), similar to results reported for heart mitochondria from guinea pigs (2.3) and rabbits (1.9)[33]. In this temperature range, Q_{10} values were close to 2.0 for NS-OXPHOS and ETS capacity, but an unexpectedly low Q_{10} of 1.4 was observed for PGM_P.

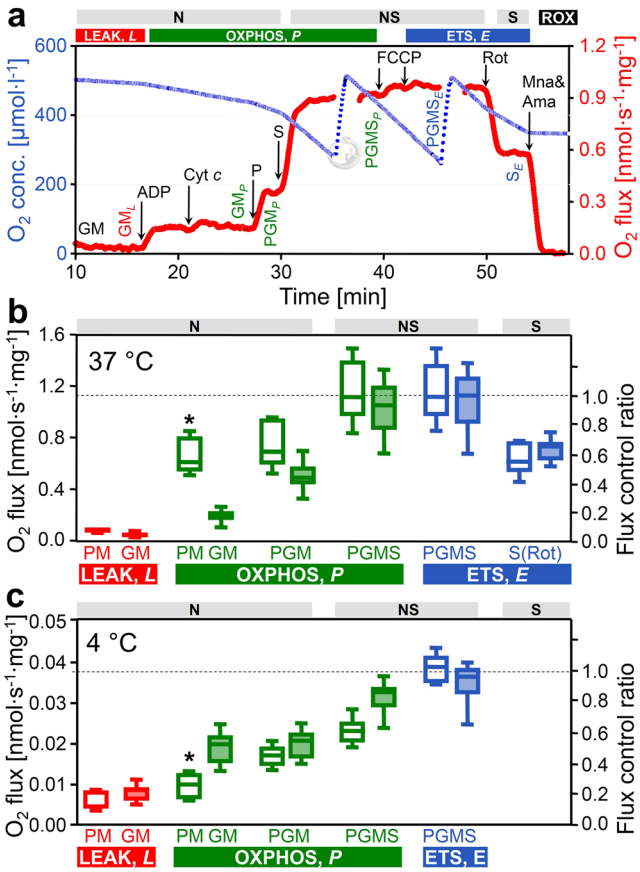

Figure 2. Respiration of permeabilized cardiac fibers (J_{O2}, per wet weight), and flux control ratios normalized for NS-ETS capacity. (**a**) Oxygen consumption measured at 37 °C in SUIT 2 protocol: GM (N-LEAK respiration; GM_L), ADP (N-OXPHOS capacity; GM_P), cytochrome *c* (integrity of outer mt-membrane), pyruvate (N-OXPHOS capacity; PGM_P), succinate (NS-OXPHOS capacity; $PGMS_P$), FCCP (NS-ETS capacity; $PGMS_E$), rotenone (Rot; inhibition of CI, S-ETS capacity; S_E), malonic acid and antimycin A (Mna and Ama; less than 2% residual oxygen consumption, ROX). (**b**,**c**) ROX-corrected respiration at 37 °C and 4 °C: LEAK respiration and OXPHOS capacity with PM (SUIT 1, open boxes, $n = 7$ and 6 at 37 and 4 °C) or GM (SUIT 2, filled boxes, $n = 16$ and 8 at 37 and 4 °C). Note the switch of the flux control pattern for N-OXPHOS capacity (PM_P vs. GM_P). The two SUIT protocols merge at state PGM_P, but results are shown separately (not significantly different). Flux control ratios are normalized relative to median $PGMS_E$ of the combined protocols. Box plots indicate the minimum, 25th percentile, median, 75th percentile, and maximum. *Significant differences between the two SUIT protocols for the same state. For abbreviations see Fig. 1.

The N/NS flux control ratio (PGM/PGMS) increased with a decrease of temperature, from 0.53 (0.40–0.69) at 37 °C to 0.66 (0.58–0.72) at 25 °C, and remained high at 0.68 (0.55–0.79) at 4 °C (Fig. 2c).

OXPHOS at 4 °C was only 3% of normothermic flux. This pronounced metabolic arrest resulted from the high thermal sensitivity of respiration with pyruvate (Table 1). Q_{10} for OXPHOS capacity with pyruvate&malate and PGMS increased up to 4 and 5 under hypothermia from 25 to 4 °C. OXPHOS capacity with glutamate&malate was much less temperature dependent, with a Q_{10} of 1.4 from 37 to 25 °C, and 2.7 from 25 to 4 °C. The OXPHOS capacity with PM was more than 2-fold higher than for GM at physiological temperature, but was depressed at 4 °C to a level even below GM-supported respiration (Fig. 2c).

Electron transfer system capacity and coupling. Uncoupler titrations were performed in the ADP-activated state, to evaluate ETS capacity (*E*, noncoupled) in relation to OXPHOS capacity (*P*, coupled). *P* and *E* were numerically almost identical, indicating that the capacity of the phosphorylation system did not exert a limiting effect on respiration, with control located mainly at the level of the dehydrogenases (Fig. 1a). LEAK respiration is an acronym for the resting oxygen flux compensating for proton leak, proton slip and cation cycling. LEAK respiration is an inverse function of the proton/electron stoichiometry[49] and is therefore higher for the S- versus N-pathway with two and three coupling sites, respectively. LEAK respiration, *L*, was measured in the presence of PM or GM before addition of ADP (N_L) and OXPHOS capacity was obtained after stimulation by ADP (N_P). OXPHOS coupling efficiencies[19], $1\text{-}L/P$, were independent of temperature in the range of 25 to 40 °C, and higher for PM than GM: 0.85 (0.78–0.89), 0.73 (0.57–0.80) and 0.82 (0.79–0.82) for PM, compared to 0.72 (0.54–0.81), 0.64 (0.39–0.89) and 0.69 (0.67–0.85) for GM at 37 °C, 30 °C, and 25 °C, respectively. At 4 °C,

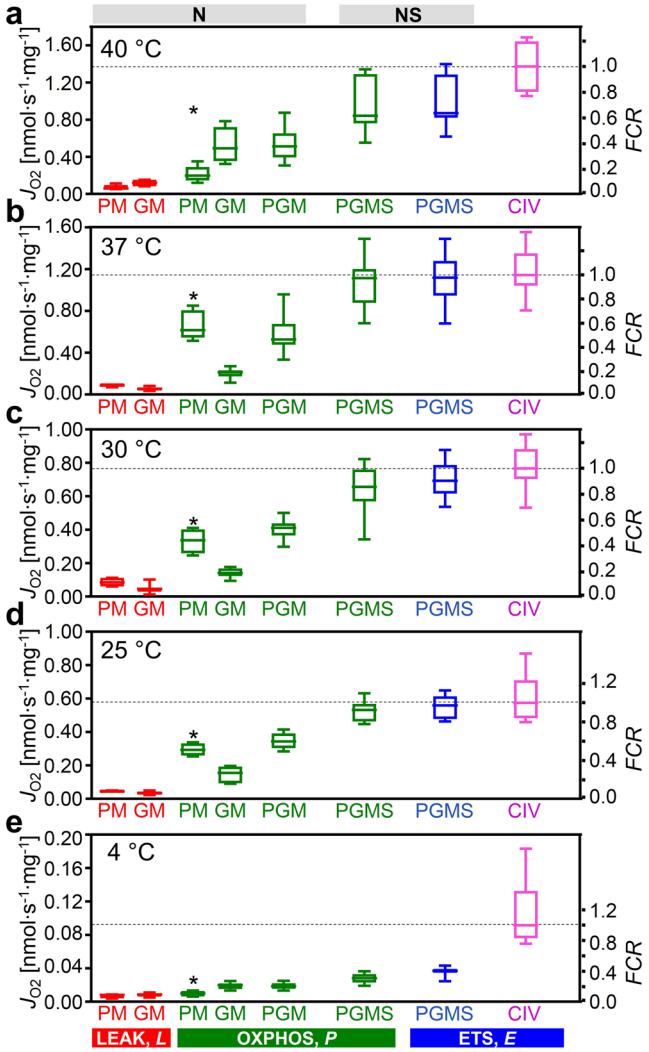

Figure 3. Respiration of permeabilized cardiac fibers (J_{O2}, per wet weight), and flux control ratios, *FCR*, normalized for CIV activity at different temperatures. N_L and N_P with PM (SUIT 1; $n = 4–7$) or GM (SUIT 2; $n = 5–16$); N_P with PGM, NS_P and NS_E with PGMS (both protocols combined; $n = 9–23$); normalized relative to median CIV_E ($n = 4–16$). *Significant differences between the two SUIT protocols for the same state. For box plots and abbreviations see Figs 1 and 2.

OXPHOS coupling efficiencies declined with GM to 0.58 (0.47–0.73), but even more with PM to 0.48 (0.28–0.60). The Q_{10} of LEAK respiration with GM and PM remained close to 2.0 down to 4 °C (Fig. 4b; triangles).

Apparent cytochrome *c* oxidase excess capacity. Since electron transfer capacity is limited when electrons are supplied only through the N-pathway, the major control resides under these conditions upstream in the dehydrogenases of the TCA cycle, with a correspondingly high apparent excess capacity of respiratory complexes downstream (for review see ref. 16). In physiological states with simultaneous NS-electron flow, the apparent excess capacity of downstream electron transfer is lower and flux control is shifted towards CIII and CIV. We therefore examined the apparent excess capacity of CIV at maximum convergent pathway flux through the ETS. Azide titrations resulted in a hyperbolic inhibition of CIV (Fig. 5a–e). The threshold plots display NS-pathway flux as a function of CIV activity (Fig. 5f–j). The two distinct phases are related to (1) the elimination of excess capacity above the threshold (initial slope; dotted lines) and (2) the flux control coefficient below the threshold, where further inhibition of CIV causes a linear inhibition of pathway flux (full lines). Inhibition of CIV activity to 41% of controls exerted only a minor effect on respiratory capacity (37 °C; Fig. 5g). The apparent excess capacity of CIV, j_{ExCIV} (for definition see Fig. 5), at 37 °C was significant (median 0.72, range 0.28–1.11) with reference to convergent NS-electron flow, which provides the basis for a low flux control coefficient of CIV and a high functional threshold (Fig. 5g). CIV excess capacities based on threshold plots were 0.6 to 0.8 at 40 to 25 °C (Fig. 5f–i). The steep increase of j_{ExCIV} to 6.2 at 4 °C (Fig. 5j) was associated with the high temperature sensitivity of ETS capacity upstream of CIV (Fig. 3e).

State		Q_{10} (x *MF*) from T_1 to T_2			
		4 °C to 25 °C	25 °C to 37 °C	30 °C to 37 °C	37 °C to 40 °C
CIV_{E0}	extrapolated	1.84 (x 3.61)	1.66 (x 1.83)	2.17 (x 1.72)	0.39 (x 0.76)
CIV_E	measured	2.40 (x 6.27)	1.77 (x 1.99)	1.77 (x 1.49)	1.84 (x 1.20)
NS_E	$PGMS_E$	3.64 (x 15.1)	1.78 (x 2.00)	1.98 (x 1.61)	0.43 (x 0.78)
NS_P	$PGMS_P$	4.06 (x 19.0)	1.85 (x 2.10)	2.13 (x 1.70)	0.39 (x 0.76)
S_E	PGMS $(Rot)_E$	—	1.93 (x 2.20)	2.19 (x 1.73)	0.25 (x 0.66)
N_P	PGM_P	4.03 (x 18.7)	1.42 (x 1.53)	1.43 (x 1.28)	0.91 (x 0.97)
N_P	PMc_P	5.01 (x 29.5)	1.86 (x 2.10)	2.36 (x 1.82)	0.48 (x 0.80)
N_P	PM_P	4.24 (x 20.7)	1.95 (x 2.22)	2.39 (x 1.84)	0.55 (x 0.84)
N_P	GMc_P	2.67 (x 7.85)	1.29 (x 1.36)	1.79 (x 1.51)	0.78 (x 0.93)
N_P	GM_P	2.49 (x 6.81)	1.39 (x 1.48)	2.07 (x 1.67)	0.65 (x 0.88)
N_L	PM_L	2.23 (x 5.41)	1.76 (x 1.97)	1.01 (x 1.01)	3.13 (x 1.41)
N_L	GM_L	1.93 (x 3.99)	1.45 (x 1.54)	1.23 (x 1.16)	1.38 (x 1.10)

Table 1. Effect of temperature on mitochondrial respiration as a function of metabolic state in permeabilized mouse heart fibers. Q_{10} is the multiplication factor for an increase by 10 °C, calculated for respiratory flux, J, in the experimental temperature intervals, T_1 to T_2. Numbers in parentheses are multiplication factors ($MF = J_{T2}/J_{T1}$) to convert J from T_1 to T_2. Q_{10} and MF are medians ($n = 4$–16). $Q_{10} = MF \exp(10/(T_2 - T_1))$. Cytochrome *c* oxidase activity was measured with 2 mM ascorbate and 500 µM TMPD (CIV_E) or extrapolated from threshold plots (CIV_{E0}; Fig. 5). For abbreviations see Figs 1 and 2.

Discussion

Mitochondrial respiration in the living cell is supported by fuel substrates supplying electrons to multiple dehydrogenases followed by convergent electron entry into the Q-junction. Physiological respiratory capacity is underestimated in isolated mitochondria and permeabilized fibers when using simple substrate combinations such as pyruvate&malate supporting the NADH-pathway (N), or a single substrate for the succinate-pathway (S). N-OXPHOS capacity ($PGM_P = 0.52$ nmol $O_2 \cdot s^{-1}$ mg^{-1} wet weight) from the present study of permeabilized cardiac fibers of the mouse (Fig. 2b), is in the same order of magnitude as *ex vivo* maximal myocardial oxygen consumption measured with cardiac perfusion after stimulation to maximal workload (0.2–0.7 nmol $O_2 \cdot s^{-1}$ mg^{-1} wet weight)[50,51]. However, PGM_P reached only 54% of NS-OXPHOS capacity ($PGMS_P = 1.02$ nmol $O_2 \cdot s^{-1} \cdot mg^{-1}$ wet weight), which actually exceeds maximal oxygen consumption of the perfused working heart. Similarly, oxygen consumption of the perfused dog heart has been compared with N-OXPHOS capacity of isolated mitochondria expressed per tissue mass (0.42 and 0.50 nmol $O_2 \cdot s^{-1}$ mg^{-1} wet weight, respectively)[52]. Under conditions of separate N- or S-pathway control, flux is limited artificially by selective substrate supply and electron gating, thus effectively under-utilizing the apparent excess capacity of respiratory complexes downstream[19] and shifting flux control to dehydrogenases upstream[53]. As expected on the basis of this respiratory flux control pattern, the artificial excess capacity of CIV with respect to N-OXPHOS capacity is high (2.2; unpublished observation), similar to artificial CIV excess capacities in permeabilized fibers from human skeletal muscle[54] and isolated mitochondria from rat heart and skeletal muscle (1.0 to 2.0)[55,56]. Our data provide a rationale suggesting that these high apparent CIV excess capacities represent *in vitro* experimental artifacts which can be easily avoided. The additive effect of convergent electron flow has profound consequences for optimization of mitochondrial respiratory control. The apparent CIV excess capacity was lower when related to maximum ETS capacity of the NS-pathway (0.7 at 37 °C; Fig. 5), consistent with apparent CIV excess capacities in intact, uncoupled cells (0.0 to 0.4)[57–59] and permeabilized human skeletal muscle fibers with NS-pathway control (0.4)[54]. Therefore, previously suggested discrepancies of CIV excess capacities in isolated mitochondria versus permeabilized fibers or intact cells[54,57,58] can be explained by NS- versus N- or S-pathway control states in mt-preparations and the concept of the Q-junction. Rocher *et al.*[60] indicated that the quantity of mtDNA in human cell lines is tightly correlated to CIV activity. Importantly, apparent excess of catalytic capacity does not signify that it is not functionally required, considering the importance for high affinity of mitochondria to oxygen[55,61] and the role of CIV in the control of cytochrome reduction levels[62].

Respiratory complexes form supercomplexes modulated by assembly factors, contributing to respiratory control and optimization of cellular metabolism[63]. Electrons are channeled through supercomplexes (CI + III and CI + III + IV in the mouse heart)[64,65] which restrict exchange with the free Q- and cytochrome *c*-pools, thus limiting random collisions[64,66,67]. Under conditions of tight electron channeling, activation of an additional convergent pathway would exert a completely additive effect on ETS capacity. Our results provide evidence against maximally tight supercomplex channeling in the mouse heart, since the combined NS-pathway capacity was significantly less than predicted from a completely additive effect of the N- and S-pathway fluxes measured separately. Two other mechanisms could reduce the additive effect on ETS capacity: (i) substrate competition for transport across the inner mt-membrane[31], and (ii) limitation of electron transfer by deficient enzyme capacities downstream of the Q-cycle in the absence of tight channeling. The additive effect on flux of convergent electron transfer at the Q-junction varies between species, strains, tissues, age, and pathophysiological conditions, unraveling an unexpected diversity of mitochondrial respiratory control patterns[28].

The phosphorylation system represents another functional unit potentially contributing to the limitation of OXPHOS capacity, *P*, relative to ETS capacity, *E*. The extent of this limitation, $E - P$, is expressed by the excess

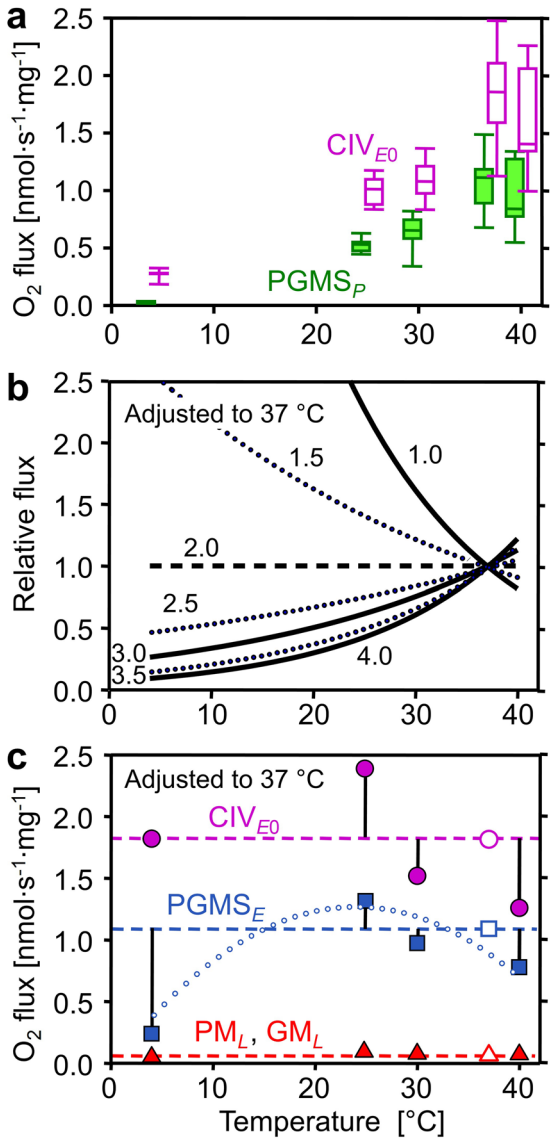

Figure 4. Effect of temperature on mitochondrial respiration. (**a**) Mass-specific oxygen flux (J_{O2}) in respiratory states $PGMS_P$ (filled boxes) and CIV_{E0} extrapolated from the threshold plots in Fig. 5 (empty boxes). (**b**) Respiratory flux (j_{O2}) relative to a simple temperature reference model: the reference flux is defined at 37 °C as 1.0 and at other temperatures as 1.0 if Q_{10} is constant at 2.0 (horizontal dashed line). Non-linear deviations from standard conditions (full and dotted lines) are obtained when Q_{10} differs from 2.0 (Q_{10} shown by numbers) and is constant throughout the entire temperature range. (**c**) j_{O2} relative to standard temperature correction of flux at 37 °C ($Q_{10} = 2.0$; horizontal lines): CIV_{E0} (● extrapolated from the threshold plots, Fig. 5), ETS capacity (■ $PGMS_E$), and LEAK respiration (▲ pooled GM_L and PM_L). Vertical bars show deviations of experimental results (means, $n = 5$ to 14) from the theoretical line for a Q_{10} of 2.0. The dotted trend line illustrates the change of temperature sensitivity for ETS, particularly at 4 °C. For box plots and abbreviations see Figs 1 and 2.

$E-P$ capacity factor, $j_{ExP} = (E-P)/E = 1 - P/E$, ranging from zero (no limitation) to the upper limit of 1.0[19]. j_{ExP} was very low but significantly different from zero in mouse heart (0.03 at 25, 37, and 40 °C, and 0.05 at 30 °C; $P < 0.05$, pooled protocols; Fig. 3), while it is zero in mouse skeletal muscle[27] and rat heart[23], and 0.04 and 0.02 in rat soleus and extensor digitorum longus muscle, respectively[26]. In human skeletal muscle, however, the limitation by the phosphorylation system is highly significant, $j_{ExP}(NS) = 0.05$ to 0.2[7,68] and $j_{ExP}(N) = 0.2$ with glutamate&malate as substrates[69], and is even more pronounced in the human heart, with $j_{ExP}(N)$ increasing from 0.52 in healthy controls to 0.59 in heart failure[2].

Temperature exerts complex effects on coupling control of mitochondrial respiration[70]. Proton leak is a property of the inner mt-membrane and depends on mt-membrane potential, whereas proton slip is a property of the proton pumps and depends on enzyme turnover. Fierce controversies on proton leak versus slip, which collectively control LEAK respiration, could be resolved by considering physiological (37 °C) versus conventional 'bioenergetic' temperature (25 °C)[70]. Temperature coefficients vary between different enzyme-catalyzed reactions involved in mitochondrial respiration (Table 1). Relatively small differences of Q_{10} among the different enzymes

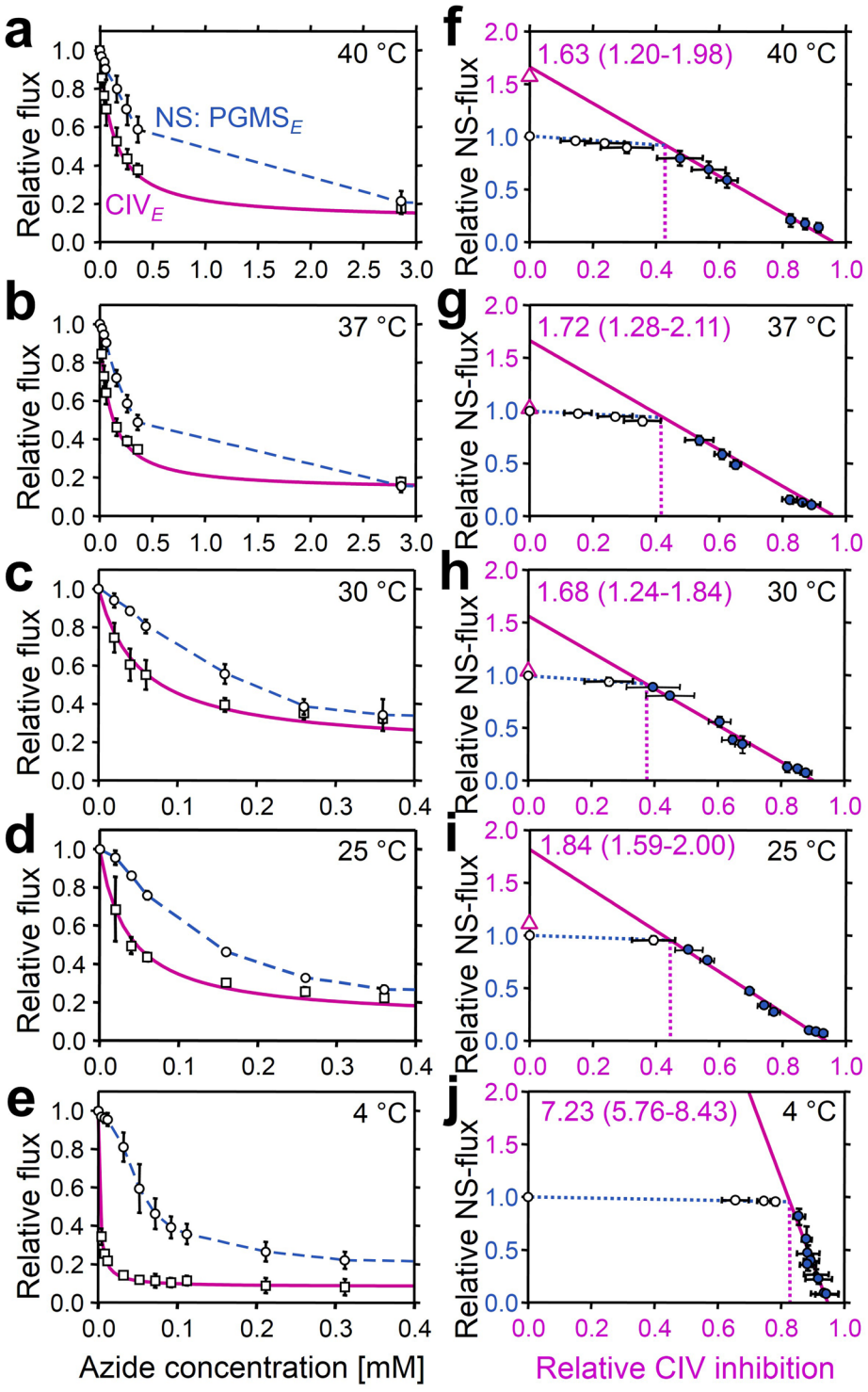

Figure 5. Azide titration and Complex IV threshold in permeabilized cardiac fibers at 40 to 4 °C. (**a** to **e**) Effect of azide titration on relative NS-pathway ETS capacity ($PGMS_E$; circles, dashed line: linear interpolations) and velocity of the single enzyme cytochrome *c* oxidase (CIV_E; squares, solid line: hyperbolic fit). (**f** to **j**) Threshold plots of relative NS-pathway flux as a function of relative inhibition of CIV at identical azide concentrations. Data up to the threshold of inhibition are shown by open symbols. The CIV_{E0}/NS_E flux ratio is calculated as the intercept at zero CIV inhibition of a linear regression through the data above the inflection point (closed symbols; $r^2 \geq 0.99$). CIV_{E0}/NS_E values are listed in the graphs as medians (min to max). The apparent excess capacity of CIV is $j_{ExCIV} = CIV_{E0}/NS_E - 1$. Triangles on *Y* axes show medians of relative CIV activities measured directly with ascorbate and TMPD ($CIV_E/NS_E = 3.0$ at 4 °C; not shown). The threshold of inhibition is at the intercept between the linear regression and the extrapolated line drawn from the control to the first inhibited flux (dotted vertical lines). Circles are means ± SD ($n = 4$–5).

of a pathway may have dramatic impact on metabolic organization and OXPHOS remodeling over a wide range of temperatures. The excess $E-P$ capacity factor in the mouse heart increased at 4 °C to 0.36 (0.33–0.51) and 0.09 (0.03–0.16) in SUIT 1 and 2, respectively (Fig. 2c), consistent with an increase of the flux control coefficient of the phosphorylation system at low temperature in rat liver mitochondria[70,71]. Furthermore, the apparent CIV excess capacity in mouse heart increased strikingly at 4 °C compared to normothermic values (Fig. 5). The excess of CIV relative to NS-pathway capacity increases in peritoneal but not in alveolar murine macrophage-derived cell lines at 25 °C compared to 37 °C[72]. Although a decline of CI activity with temperature is possibly involved in the shift of CIV excess capacity[72], our results suggest a different mechanism. The highest OXPHOS Q_{10} of 5.0 was obtained with pyruvate&malate between 4 and 25 °C, in contrast to the lower Q_{10} with glutamate&malate (Table 1). Both substrate combinations fuel the N-pathway with electron entry into the Q-junction through CI. Hence the activities of CI and downstream respiratory complexes cannot explain the observed hypothermic response pattern. The most likely candidates responsible for the high temperature sensitivity of the pyruvate&malate pathway, therefore, are pyruvate dehydrogenase, the pyruvate transporter and possibly citrate synthase. This is supported by a previous study on rat heart mitochondria showing a high thermal sensitivity of pyruvate-supported respiration and activity of pyruvate dehydrogenase at low temperature[73].

The thermal sensitivity of pyruvate supported respiration was not as pronounced in a cold adapted fish species (*Anarhicas lupus*)[74], suggesting that pyruvate dehydrogenase plays not only an important role in the response of OXPHOS to temperature in the murine heart[73], but is also a potential site of key adaptation to upgrade mitochondrial capacity at low temperature in ectotherm species[75]. This is in line with evidence of control of convergent OXPHOS at upstream steps of electron supply in *Fundulus heteroclitus* heart mitochondria[76,77]. A higher control of the phosphorylation system is observed at lower temperature (17 °C compared to 25 °C) in permeabilized heart fibers from the triplefin fish (*Forsterygion lapillum*)[78]. N- or S-pathway capacity appeared to be more affected by temperature changes at lower temperature compared to CIV in the freshwater turtle *Trachemys scripa*[79]. Similarly, permeabilized muscle fibers from *Drosophila simulans* show an increase of CIV excess capacity at low temperature[80]. Taken together, NADH-linked mt-matrix dehydrogenases and the phosphorylation system rather than electron transfer complexes appear to be the primary modulators of respiratory control patterns at low temperature in mitochondria from endotherm and ectotherm species.

The conventional respiratory acceptor control ratio, RCR (State 3/State 4 or P/L ratio)[20] was 6.7 with PM (37 °C), and much lower (3.6) with GM. For statistical and conceptual reasons, the RCR is replaced by the OXPHOS coupling efficiency[19], $1-L/P = 1\text{-RCR}^{-1}$. The low OXPHOS coupling efficiency for GM of 0.72 (compared to 0.85 for PM) reflects the low OXPHOS capacity supported by specific substrates, rather than low coupling efficiency. Evaluation of coupling must be based on pathway control states supporting a high ETS capacity under conditions not limited by substrates or by the phosphorylation system. Hence, pyruvate&malate supporting a 'fast' N-pathway at 37 °C yields a more appropriate index of coupling. Under deep hypothermia (4 °C), however, estimation of coupling is complicated by the strong thermal sensitivity of ETS capacity compared to LEAK respiration (Fig. 3b) and by the limitation imposed on OXPHOS capacity by the phosphorylation system.

Our results imply that relevant experimental models of pathophysiological metabolic states can be established by reconstitution of bioenergetic pathways in mitochondrial preparations[19]. In addition to the core bioenergetic N- and S-pathway, fatty acid oxidation contributes to convergent electron flow to the Q-junction through the electron transferring flavoprotein complex[2,19] (Fig. 1). In human hearts, ATP demand is fueled up to 50–70% by fatty acid oxidation, predominating over glucose oxidation (see review[81]). The temperature dependence of substrate competition versus additivity of mitochondrial fatty acid and glucose-linked oxidative capacity, therefore, will represent an important extension of the present study. In addition, the convergent glycerophosphate pathway (Fig. 1) and the malate-aspartate shuttle play key roles in linking the redox biochemistry of the cytosolic and mitochondrial compartments. Mapping the additive effects of convergent bioenergetic pathways on respiratory capacities sets the stage to integrate further analyses of respiratory states (mitochondrial membrane potential, cytochrome redox states[82]) and generation of reactive oxygen species into a systems analysis of mitochondrial respiratory control.

Estimation of maximal respiratory capacity should be performed at physiological temperature and with substrate combinations appropriate to ensure suitable operation of the TCA cycle and multiple entries of electrons into the Q-cycle. Those conditions define the physiological reference state for mitochondrial respiratory control. This is of major significance to better explain the pathological effects of genetic mutations and acquired CIV deficiencies. Furthermore, our results on the key modulators of thermal sensitivity of mitochondrial metabolism will allow to determine how cells and tissues are impaired by temperature changes, including mild to deep hypothermia in cardiac surgery. This novel aspect of mitochondrial medicine may provide a basis for intervention strategies to limit damages[72]. Consideration of a standardized nomenclature for categories of hypothermia will improve conceptually the experimental design and reporting in the mitochondrial field, and facilitate translational research from mitochondrial physiology to the clinic[34]. Application of comprehensive OXPHOS analysis for diagnosis of mitochondrial preservation will contribute to optimize the degree of therapeutic hypothermia in the clinical setting, including cardiac arrest during surgery and resuscitation[83,84]. From an evolutionary perspective, our study allows to pinpoint candidate loci that are potentially under selective pressure and therefore represent targets for seeking mechanisms of adaptation to different temperature regimes. In summary, we propose the hypothesis that the likely modulators of adaptation and acclimatization to low temperature are compensatory mechanisms to counteract upstream limitations of ETS capacity at the entry to and within the TCA cycle (particularly pyruvate dehydrogenase) and downstream limitation of flux by the phosphorylation system.

Methods

Preparation of permeabilized fibers. Adult male mice C57 BL/6 N were housed under standard conditions according to the Austrian Animal Care Law. At 8 to 10 weeks of age (23 ± 3 g), animals were anaesthetized with ketamine and xylazine (80 and 10 mg·kg^{-1}, respectively) given intramuscularly and checked for absence of the toe-pinch reflex before performing a cervical dislocation. The heart was excised and placed in 5 ml of ice-cold relaxing solution BIOPS[2]. After rapid mechanical permeabilization of the left ventricle (~40 mg wet weight), bundles of fibers were agitated gently (30 min, 4 °C) in BIOPS supplemented with 50 µg·ml^{-1} saponin[85]. Fibers were washed by agitation (10 min, 4 °C) in mitochondrial respiration medium MiR05[42], immediately blotted, weighed, and used for respirometric measurements.

High-resolution respirometry. Respiration was measured simultaneously in 10 respiration chambers (O2k; Oroboros Oxygraph-2k, Innsbruck, Austria), one O2k with two chambers for each of the following temperatures: 4, 25, 30, 37, and 40 °C. Permeabilized fibers (0.7–1.3 mg at 25 to 40 °C and 7–8 mg at 4 °C) were used in each chamber containing 2 ml of MiR05. Respiratory flux was expressed per mg wet weight of fibers. Instrumental and chemical oxygen background fluxes were calibrated as a function of oxygen concentration and subtracted from the total volume-specific oxygen flux (Datlab software, Oroboros Instruments)[55,82,86]. An oxygen regime of 500 to >200 µM was maintained at 30 to 40 °C, but up to 700 and 900 µM at 25 and 4 °C, to avoid artificial oxygen diffusion limitation of flux[86,87]. In the first substrate-uncoupler-inhibitor titration protocol (SUIT 1), the following final concentrations were added sequentially: P (5 mM), M (5 mM), G (10 mM), ADP (1 mM), cytochrome *c* (10 µM), S (10 mM), FCCP (carbonyl cyanide *p*-trifluoromethoxyphenylhydrazone; optimum concentration, 0.125 to 0.375 µM), rotenone (Rot; 0.5 µM), antimycin A (Ama; 2.5 µM), malonic acid (Mna; 5 mM), ascorbate (As; 0.5 mM) and TMPD (*N*,*N*,*N*',*N*'-tetramethyl-*p*-phenylenediamine; 2 mM). In SUIT 2 addition of P and G were inversed (Fig. 1b). An increase of respiration due to cytochrome *c* addition after ADP was observed at 30 to 40 °C, with cytochrome *c* control factors (change of respiration divided by cytochrome *c* stimulated respiration)[19] in the range of 0.05 to 0.15, with higher values of 0.11 to 0.20 at 25 °C. At 4 °C, N-OXPHOS capacity showed a trend to decline during the experiment particularly with PM, and no stimulation could be observed with cytochrome *c*. Thus the integrity of the outer mitochondrial membrane in mouse heart permeabilized fibers was comparable to rat heart fibers studied at 30 °C[88]. Residual oxygen consumption (ROX), evaluated after inhibition of CI, CII and CIII with Rot, Mna and Ama was a small fraction (0.01 to 0.02) of NS-ETS capacity at 25 to 40 °C, but increased to 0.04 to 0.10 at 4 °C. Nevertheless, correction of fluxes in all respiratory states for ROX was significant, particularly in the resting state of LEAK respiration, when ROX was as high as 0.12 to 0.32 of total oxygen consumption in the N-LEAK state at 25 to 40 °C.

Apparent CIV excess capacities were determined by azide titrations of CIV activity and of NS-ETS capacity at 4, 25, 30, 37, and 40 °C. Threshold plots of relative respiration rate against the fraction of inhibited CIV activity at the same azide concentration were made as previously described[57,89]. Azide titrations were performed at optimum uncoupler concentration supporting maximum flux, preventing the effect of inhibition of ATP synthase[90] and eliminating any contribution of the phosphorylation system to flux control. The following azide concentrations were used [mM]: 0.02, 0.04, 0.06, 0.16, 0.26, 0.36, 2.9, 5.4, 10.4 between 25 and 40 °C, and 0.004, 0.008, 0.012, 0.032, 0.052, 0.072, 0.092, 0.11, 0.21, 0.31, 2.8, 5.3, 10.3 at 4 °C (not all points visible in Fig. 5 due to overlap).

The contents of the chambers were removed at the end of each experimental run and the chamber was rinsed twice with 500 µl of respiration medium. The fibers were homogenized for 2 × 30 s with an Ultra-Turrax homogenizer at maximum speed and immediately frozen in liquid nitrogen and stored at −80 °C for subsequent measurement of citrate synthase at 30 °C[91].

Statistical analysis. Statistica software© was used for statistical analyses. Data were log transformed to meet the requirement for heteroscedasticity according to Levene's test. A three-factor ANOVA (protocol, state and temperature) followed by *a posteriori* Tukey multiple comparison tests were used to test for differences between protocols at a specific state and temperature. To determine the effects of addition of substrates, cytochrome *c*, inhibitors, or uncoupler, a t-test for dependent samples was used. Significance was considered at $P < 0.05$. Results are presented without transformation as medians (min-max) unless specified otherwise.

References

1. Schwerzmann, K., Hoppeler, H., Kayar, S. R. & Weibel, E. R. Oxidative capacity of muscle and mitochondria: Correlation of physiological, biochemical, and morphometric characteristics. *Proc. Natl. Acad. Sci. USA* **86**, 1583–1587, doi:10.1073/pnas.86.5.1583 (1989).
2. Lemieux, H., Semsroth, S., Antretter, H., Höfer, D. & Gnaiger, E. Mitochondrial respiratory control and early defects of oxidative phosphorylation in the failing human heart. *Int. J. Biochem. Cell Biol.* **43**, 1729–1738, doi:10.1016/j.biocel.2011.08.008 (2011).
3. Li, P. *et al.* Mitochondrial respiratory dysfunctions of blood mononuclear cells link with cardiac disturbance in patients with early-stage heart failure. *Sci. Rep.* **5**, 10229, doi:10.1038/srep10229 (2015).
4. Marín-García, J. *Mitochondria and the heart* (Springer Science+Business Media, Inc., 2005).
5. Kuznetsov, A. V. *et al.* Mitochondrial defects and heterogeneous cytochrome *c* release after cardiac cold ischemia and reperfusion. *Am. J. Physiol.-Heart Circul. Physiol* **286**, H1633–H1641, doi:10.1152/ajpheart.00701.2003 (2004).
6. Schrauwen, P. & Hesselink, M. K. C. Oxidative capacity, lipotoxicity and mitochondrial damage in type 2 diabetes. *Diabetes* **53**, 1412–1417, doi:10.2337/diabetes.53.6.1412 (2004).
7. Boushel, R. *et al.* Patients with type 2 diabetes have normal mitochondrial function in skeletal muscle. *Diabetologia* **50**, 790–796, doi:10.1007/s00125-007-0594-3 (2007).
8. Bombicino, S. S. *et al.* Diabetes impairs heart mitochondrial function without changes in resting cardiac performance. *Int. J. Biochem. Cell Biol.* **S1357–2725**, 30280–30281, doi:10.1016/j.biocel.2016.09.018 (2016).
9. Warfel, J. D. *et al.* Mitochondrial fat oxidation is essential for lipid-induced inflammation in skeletal muscle in mice. *Sci. Rep.* **28**, 37941, doi:10.1038/srep37941 (2016).

10. Lesnefsky, E. J., Chen, Q. & Hoppel, C. L. Mitochondrial metabolism in aging heart. *Circ. Res.* **118**, 1593–1611, doi:10.1161/CIRCRESAHA.116.307505 (2016).
11. Martín-Fernández, B. & Gredilla, R. Mitochondria and oxidative stress in heart aging. *Age (Dordr)* **8**, 225–238, doi:10.1007/s11357-016-9933-y (2016).
12. Chinnery, P. F. & Turnbull, D. M. Clinical features, investigation, and management of patients with defects of mitochondrial DNA. *J. Neurol. Neurosurg. Psychiatry* **63**, 559–563, doi:10.1136/jnnp.63.5.559 (1997).
13. von Kleist-Retzow, J. C., Schauseil-Zipf, U., Michalk, D. V. & Kunz, W. S. Mitochondrial diseases - an expanding spectrum of disorders and affected genes. *Exp. Physiol.* **88**, 155–166, doi:10.1113/eph8802509 (2003).
14. Wallace, D. C. Mitochondrial defects in cardiomyopathy and neuromuscular disease. *Am. Heart J.* **139**, S70–85, doi:10.1067/mhj.2000.103934 (2000).
15. Sameni, S., Syed, A., Marsh, J. L. & Digman, M. A. The phasor-FLIM fingerprints reveal shifts from OXPHOS to enhanced glycolysis in Huntington Disease. *Sci. Rep.* **6**, 4755, doi:10.1038/srep34755 (2016).
16. Rossignol, R. *et al*. Mitochondrial threshold effects. *Biochem. J.* **370**, 751–762, doi:10.1042/bj20021594 (2003).
17. Gertz, E. W., Wisneski, J. A., Stanley, W. C. & Neese, R. A. Myocardial substrate utilization during exercise in humans. Dual carbon-labeled carbohydrate isotope experiments. *J. Clin. Invest.* **82**, 2017–2025, doi:10.1172/JCI113822 (1988).
18. van der Vusse, G. J., Glatz, J. F., Stam, H. C. & Reneman, R. S. Fatty acid homeostasis in the normoxic and ischemic heart. *Physiol. Rev.* **72**, 881–940 (1992).
19. Gnaiger, E. Mitochondrial pathways and respiratory control. An introduction to OXPHOS analysis. 4th ed. Mitochondr Physiol Network 19.12. *OROBOROS MiPNet Publications*, Innsbruck, 80 pp (2014).
20. Chance, B. & Williams, G. R. Respiratory enzymes in oxidative phosphorylation. I. Kinetics of oxygen utilization. *J. Biol. Chem.* **217**, 383–393 (1955).
21. Estabrook, R. Mitochondrial respiratory control and the polarographic measurement of ADP:O ratios. *Methods Enzymol.* **10**, 41–47, doi:10.1016/0076-6879(67)10010-4 (1967).
22. Costa, L. E., Boveris, A., Koch, O. R. & Taquini, A. C. Liver and heart mitochondria in rats submitted to chronic hypobaric hypoxia. *Am. J. Physiol.-Cell Physiol.* **255**, C123–C129 (1988).
23. Lemieux, H., Vazquez, E. J., Fujioka, H. & Hoppel, C. L. Decrease in mitochondrial function in rat cardiac permeabilized fibers correlates with the aging phenotype. *J. Gerontol. A. Biol. Sci. Med. Sci.* **65**, 1157–1164, doi:10.1093/gerona/glq141 (2010).
24. Garait, B. *et al*. Fat intake reverses the beneficial effects of low caloric intake on skeletal muscle mitochondrial H_2O_2 production. *Free Radic. Biol. Med.* **39**, 1249–1261, doi:10.1016/j.freeradbiomed.2005.06.026 (2005).
25. Llesuy, S. *et al*. Oxidative stress in muscle and liver of rats with septic syndrome. *Free Rad. Biol. Med.* **16**, 445–451, doi:10.1016/0891-5849(94)90121-X (1994).
26. Warren, B. E. *et al*. Early mitochondrial dysfunction in glycolytic muscle, but not oxidative muscle, of the fructose-fed insulin-resistant rat. *Am. J. Physiol. Endocrinol. Metab.* **306**, E658–E667, doi:10.1152/ajpendo.00511.2013 (2014).
27. Aragonés, J. *et al*. Deficiency or inhibition of oxygen sensor Phd1 induces hypoxia tolerance by reprogramming basal metabolism. *Nat. Genet.* **40**, 170–180, doi:10.1038/ng.2007.62 (2008).
28. Gnaiger, E. Capacity of oxidative phosphorylation in human skeletal muscle. New perspectives of mitochondrial physiology. *Int. J. Biochem. Cell. Biol.* **41**, 1837–1845, doi:10.1016/j.biocel.2009.03.013 (2009).
29. Jackman, M. R. & Willis, W. T. Characteristics of mitochondria isolated from type I and type IIb skeletal muscle. *Am. J. Physiol.-Cell Physiol.* **39**, C673–C678 (1996).
30. Pecina, P. *et al*. Noninvasive diagnostics of mitochondrial disorders in isolated lymphocytes with high resolution respirometry. *Biochim. Biophys. Acta Clinical* **2**, 62–71, doi:10.1016/j.bbacli.2014.09.003 (2014).
31. Haslam, J. M. & Krebs, H. A. Substrate competition in the respiration of animal tissues. The metabolic interactions of pyruvate and alpha-oxoglutarate in rat liver homogenates. *Biochem. J.* **86**, 432–446, doi:10.1042/bj0860432 (1963).
32. N'Guessan, B. *et al*. Evaluation of quantitative and qualitative aspects of mitochondrial function in human skeletal and cardiac muscles. *Mol. Cell. Biochem.* **256**, 267–280, doi:10.1023/B:MCBI.0000009874.14649.ca (2004).
33. Lindenmayer, G. E., Sordahl, L. A. & Schwartz, A. Reevaluation of oxidative phosphorylation in cardiac mitochondria from normal animals and animals in heart failure. *Circ. Res.* **23**, 439–450, doi:10.1161/01.RES.23.3.439 (1968).
34. Yan, T. D. *et al*. Consensus on hypothermia in aortic arch surgery. *Ann. Cardiothorac. Surg.* **2**, 163–168, doi:10.3978/j.issn.2225-319X.2013.03.03 (2013).
35. Hale, S. L. & Kloner, R. A. Myocardial hypothermia: A potential therapeutic technique for acute regional myocardial ischemia. *J. Cardiovasc. Electrophysiol.* **10**, 405–413, doi:10.1111/jce.1999.10.issue-3 (1999).
36. Ning, X. H. & Chen, S. H. Mild hypothermic cross adaptation resists hypoxic injury in hearts: A brief review. *Chin. J. Physiol.* **49**, 213–222 (2006).
37. Schwartz, D. S. *et al*. Regional topical hypothermia of the beating heart: preservation of function and tissue. *Ann. Thorac. Surg.* **72**, 804–809, doi:10.1016/S0003-4975(01)02822-3 (2001).
38. Tissier, R. *et al*. Rapid cooling preserves the ischaemic myocardium against mitochondrial damage and left ventricular dysfunction. *Cardiovasc. Res.* **83**, 345–353, doi:10.1093/cvr/cvp046 (2009).
39. Huang, C. H. *et al*. Activation of mitochondrial STAT-3 and reduced mitochondria damage during hypothermia treatment for post-cardiac arrest myocardial dysfunction. *Basic Res. Cardiol.* **110**, 59, doi:10.1007/s00395-015-0516-3 (2015).
40. Jahania, M. S., Sanchez, J. A., Narayan, P., Lasley, R. D. & Mentzer, R. M. J. Heart preservation for transplantation: principles and strategies. *Ann. Thorac. Surg.* **68**, 1983–1987, doi:10.1016/S0003-4975(99)01028-0 (1999).
41. Schipper, D. A. *et al*. The Critical Role of Bioenergetics in Donor Cardiac Allograft Preservation. *J. Cardiovasc. Transl. Res.* **9**, 176–183, doi:10.1007/s12265-016-9692-2 (2016).
42. Gnaiger, E. *et al*. In *Life in the cold* (eds G. Heldmaier & M. Klingenspor) 431–442 (Springer Berlin Heidelberg, 2000).
43. Digerness, S. B. & Reddy, W. J. The malate-aspartate shuttle in heart mitochondria. *J. Mol. Cell. Cardiol.* **8**, 779–785, doi:10.1016/0022-2828(76)90084-5 (1976).
44. Lemieux, H. *et al*. Mitochondrial function is altered in horse atypical myopathy. *Mitochondrion* **30**, 35–41, doi:10.1016/j.mito.2016.06.005 (2016).
45. Winkler-Stuck, K. *et al*. Re-evaluation of the dysfunction of mitochondrial respiratory chain in skeletal muscle of patients with Parkinsons disease. *J. Neural Transm.* **112**, 499–518, doi:10.1007/s00702-004-0195-y (2005).
46. Lemasters, J. J. The ATP-to-oxygen stoichiometries of oxidative phosphorylation by rat liver mitochondria. *J. Biol. Chem.* **259**, 13123–13130 (1984).
47. Rasmussen, H. N. & Rasmussen, U. F. Small scale preparation of skeletal muscle mitochondria, criteria of integrity, and assays with reference to tissue function. *Mol. Cell. Biochem.* **174**, 55–60, doi:10.1023/A:1006851705996 (1997).
48. Rasmussen, U. F. *et al*. Aerobic metabolism of human quadriceps muscle: *in vivo* data parallel measurements on isolated mitochondria. *Am. J. Physiol.-Endocrinol. Metab.* **280**, E301–E307 (2001).
49. Brand, M. D., Chien, L. F., Ainscow, E. K., Rolfe, D. F. & Porter, R. K. The causes and functions of mitochondrial proton leak. *Biochim. Biophys. Acta* **1187**, 132–139, doi:10.1016/0005-2728(94)90099-X (1994).
50. Yan, J. *et al*. Increased glucose uptake and oxidation in mouse hearts prevent high fatty acid oxidation but cause cardiac dysfunction in diet-induced obesity. *Circulation* **119**, 2818–2828, doi:10.1161/CIRCULATIONAHA.108.832915 (2009).

51. Boudina, S. *et al*. Reduced mitochondrial oxidative capacity and increased mitochondrial uncoupling impair myocardial energetics in obesity. *Circulation* **112**, 2686–2695, doi:10.1161/CIRCULATIONAHA.105.554360 (2005).
52. Mootha, V. K., Arai, A. E. & Balaban, R. S. Maximum oxidative phosphorylation capacity of the mammalian heart. *Am. J. Physiol.-Heart Circul. Physiol.* **41**, H769–H775 (1997).
53. Ainscow, E. K. & Brand, M. D. Top-down control analysis of ATP turnover, glycolysis and oxidative phosphorylation in rat hepatocytes. *Eur. J. Biochem.* **263**, 671–685, doi:10.1046/j.1432-1327.1999.00534.x (1999).
54. Kunz, W. S. *et al*. Flux control of cytochrome c oxidase in human skeletal muscle. *J. Biol. Chem.* **275**, 27741–27745, doi:10.1074/jbc.M004833200 (2000).
55. Gnaiger, E., Lassnig, B., Kuznetsov, A., Reiger, G. & Margreiter, R. Mitochondrial oxygen affinity, respiratory flux control and excess capacity of cytochrome *c* oxidase. *J. Exp. Biol.* **201**, 1129–1139 (1998).
56. Rossignol, R., Malgat, M., Mazat, J. P. & Letellier, T. Threshold effect and tissue specificity - Implication for mitochondrial cytopathies. *J. Biol. Chem.* **274**, 33426–33432, doi:10.1074/jbc.274.47.33426 (1999).
57. Villani, G. & Attardi, G. *In vivo* control of respiration by cytochrome *c* oxidase in wild-type and mitochondrial DNA mutation-carrying human cells. *Proc. Natl. Acad. Sci. USA* **94**, 1166–1171, doi:10.1073/pnas.94.4.1166 (1997).
58. Villani, G., Greco, M., Papa, S. & Attardi, G. Low reserve of cytochrome *c* oxidase capacity *in vivo* in the respiratory chain of a variety of human cell types. *J. Biol. Chem.* **273**, 31829–31836, doi:10.1074/jbc.273.48.31829 (1998).
59. Dalmonte, M. E. *et al*. Control of respiration by cytochrome *c* oxidase in intact cells: role of the membrane potential. *J. Biol. Chem.* **284**, 32331–32335, doi:10.1074/jbc.M109.050146 (2009).
60. Rocher, C. *et al*. Influence of mitochondrial DNA level on cellular energy metabolism: implications for mitochondrial diseases. *J. Bioenerg. Biomembr.* **40**, 59–67, doi:10.1007/s10863-008-9130-5 (2008).
61. Larsen, F. J. *et al*. Mitochondrial oxygen affinity predicts basal metabolic rate in humans. *FASEB J.* **25**, 2843–2852, doi:10.1096/fj.11-182139 (2011).
62. Harrison, D. K., Fasching, M., Fontana-Ayoub, M. & Gnaiger, E. Cytochrome redox states and respiratory control in mouse and beef heart mitochondria at steady-state levels of hypoxia. *J. Appl. Physiol.* **119**, 1210–1218, doi:10.1152/japplphysiol.00146.2015 (2015).
63. Cogliati, S. *et al*. Mechanism of super-assembly of respiratory complexes III and IV. *Nature* **539**, 579–582, doi:10.1038/nature20157 (2016).
64. Bianchi, C., Genova, M. L., Castelli, G. P. & Lenaz, G. The mitochondrial respiratory chain is partially organized in a supercomplex assembly. Kinetic evidence using flux control analysis. *J. Biol. Chem.* **279**, 36562–36569, doi:10.1074/jbc.M405135200 (2004).
65. Schagger, H. & Pfeiffer, K. The ratio of oxidative phosphorylation complexes I-V in bovine heart mitochondria and the composition of respiratory chain supercomplexes. *J. Biol. Chem.* **276**, 37861–37867, doi:10.1074/jbc.M106474200 (2001).
66. Hackenbrock, C. R., Chazotte, B. & Gupte, S. S. The random collision model and a critical assessment of diffusion and collision in mitochondrial electron transport. *J. Bioenerg. Biomembr.* **18**, 331–368, doi:10.1007/BF00743010 (1986).
67. Schägger, H. Respiratory chain supercomplexes of mitochondria and bacteria. *Biochim. Biophys. Acta* **1555**, 154–159, doi:10.1016/S0005-2728(02)00271-2 (2002).
68. Pesta, D. *et al*. Similar qualitative and quantitative changes of mitochondrial respiration following strength and endurance training in normoxia and hypoxia in sedentary humans. *Am. J. Physiol. Regul. Integr. Comp. Physiol.* **301**, R1078–R1087, doi:10.1152/ajpregu.00285.2011 (2011).
69. Rasmussen, U. F. & Rasmussen, H. N. Human quadriceps muscle mitochondria: A functional characterization. *Mol. Cell. Biochem.* **208**, 37–44, doi:10.1023/A:1007046028132 (2000).
70. Dufour, S., Rousse, N., Canioni, P. & Diolez, P. Top-down control analysis of temperature effect on oxidative phosphorylation. *Biochem. J.* **314**, 743–751, doi:10.1042/bj3140743 (1996).
71. Quentin, E., Averet, N., Rigoulet, M. & Guerin, B. Temperature dependence of the coupling efficiency of rat liver oxidative phosphorylation - role of adenine nucleotide translocator. *Biochem. Biophys. Res. Commun.* **202**, 816–821, doi:10.1006/bbrc.1994.2003 (1994).
72. Groeger, M. *et al*. Temperature and cell-type dependency of sulfide effects on mitochondrial respiration. *Shock* **38**, 367–374, doi:10.1097/SHK.0b013e3182651fe6 (2012).
73. Lemieux, H., Tardif, J. C. & Blier, P. U. Thermal sensitivity of oxidative phosphorylation in rat heart mitochondria: Does pyruvate dehydrogenase dictate the response to temperature? *J. Therm. Biol.* **35**, 105–111, doi:10.1016/j.jtherbio.2009.12.003 (2010).
74. Lemieux, H., Tardif, J. C., Dutil, J. D. & Blier, P. U. Thermal sensitivity of cardiac mitochondrial metabolism in an ectothermic species from a cold environment, Atlantic wolffish (*Anarhichas lupus*). *J. Exp. Mar. Biol. Ecol.* **384**, 113–118, doi:10.1016/j.jembe.2009.12.007 (2010).
75. Blier, P. U., Lemieux, H. & Pichaud, N. Holding our breath in our modern world: will mitochondria keep the pace with global changes? *Can. J. Zool.* **92**, 591–601, doi:10.1139/cjz-2013-0183 (2014).
76. Baris, T. Z., Blier, P. U., Pichaud, N., Crawford, D. L. & Oleksiak, M. F. Gene by environmental interactions affecting oxidative phosphorylation and thermal sensitivity. *Am. J. Physiol. Regul. Integr. Comp. Physiol.* **311**, R157–R165, doi:10.1152/ajpregu.00008.2016 (2016).
77. Baris, T. Z., Crawford, D. L. & Oleksiak, M. F. Acclimation and acute temperature effects on population differences in oxidative phosphorylation. *Am. J. Physiol. Regul. Integr. Comp. Physiol* **310**, R185–R196, doi:10.1152/ajpregu.00421.2015 (2016).
78. Khan, J. R., Iftikar, F. I., Hebert, N. A., Gnaiger, E. & Hickey, A. J. Thermal plasticity of skeletal muscle mitochondrial activity and whole animal respiration in a common intertidal triplefin fish, *Forsterygion lapillum* (Family: Tripterygiidae). *J. Comp. Physiol. B* **184**, 991–1001, doi:10.1007/s00360-014-0861-9 (2014).
79. Galli, G. L. J. & Richards, J. G. The effect of temperature on mitochondrial respiration in permeabilized cardiac fibres from the freshwater turtle. *Trachemys scripta. J. Therm. Biol.* **37**, 195–200, doi:10.1016/j.jtherbio.2011.12.012 (2012).
80. Pichaud, N. *et al*. Thermal sensitivity of mitochondrial metabolism in two distinct mitotypes of *Drosophila simulans*: evaluation of mitochondrial plasticity. *J. Exp. Biol.* **213**, 1665–1675, doi:10.1242/jeb.040261 (2010).
81. Liu, Y., Neumann, D., Glatz, J. F. & Luiken, J. J. Molecular mechanism of lipid-induced cardiac insulin resistance and contractile dysfunction. *Prostaglandins Leukot Essent Fatty Acids* **S0952–3278**, 30082–30085 (2016).
82. Harrison, D. K., Fasching, M., Fontana-Ayoub, M. & Gnaiger, E. Cytochrome redox states and respiratory control in mouse and beef heart mitochondria at steady-state levels of hypoxia. *J. Appl. Physiol.* **119**, 1210–1218, doi:10.1152/japplphysiol.00146.2015 (2015).
83. Gong, P. *et al*. Hypothermia-induced neuroprotection is associated with reduced mitochondrial membrane permeability in a swine model of cardiac arrest. *J. Cereb. Blood Flow Metab.* **33**, 928–934, doi:10.1038/jcbfm.2013.33 (2013).
84. Wood, T. *et al*. Treatment temperature and insult severity influence the neuroprotective effects of therapeutic hypothermia. *Sci. Rep.* **6**, 23430, doi:10.1038/srep23430 (2016).
85. Veksler, V. I., Kuznetsov, A. V., Sharov, V. G., Kapelko, V. I. & Saks, V. A. Mitochondrial respiratory parameters in cardiac tissue: a novel method of assessment by using saponin-skinned fibers. *Biochim. Biophys. Acta* **892**, 191–196, doi:10.1016/0005-2728(87)90174-5 (1987).
86. Gnaiger, E., Steinlechner-Maran, R., Méndez, G., Eberl, T. & Margreiter, R. Control of mitochondrial and cellular respiration by oxygen. *J. Bioenerg. Biomemb.* **27**, 583–596, doi:10.1007/BF02111656 (1995).
87. Pesta, D. & Gnaiger, E. High-resolution respirometry: OXPHOS protocols for human cells and permeabilized fibers from small biopsies of human muscle. *Methods Mol. Biol.* **810**, 25–58, doi:10.1007/978-1-61779-382-0_3 (2012).

88. Kuznetsov, A. V., Brandacher, G., Steurer, W., Margreiter, R. & Gnaiger, E. Isolated rat heart mitochondria and whole rat heart as models for mitochondrial cold ischemia-reperfusion injury. *Transplant. Proc.* **32**, 45, doi:10.1016/S0041-1345(99)00869-6 (2000).
89. Letellier, T., Heinrich, R., Malgat, M. & Mazat, J. P. The kinetic basis of threshold effects observed in mitochondrial diseases - A systemic approach. *Biochem. J.* **302**, 171–174, doi:10.1042/bj3020171 (1994).
90. Bowler, M. W., Montgomery, M. G., Leslie, A. G. W. & Walker, J. E. How azide inhibits ATP hydrolysis by the F-ATPases. *Proc. Natl. Acad. Sci. USA* **103**, 8646–8649, doi:10.1073/pnas.0602915103 (2006).
91. Srere, P. A. Citrate synthase. *Methods Enzymol.* **13**, 3–11, doi:10.1016/0076-6879(69)13005-0 (1969).
92. Fang, J. *et al*. Dihydro-orotate dehydrogenase is physically associated with the respiratory complex and its loss leads to mitochondrial dysfunction. *Biosci. Rep.* **33**, e00021, doi:10.1042/BSR20120097 (2013).
93. Bouillaud, F. & Blachier, F. Mitochondria and sulfide: a very old story of poisoning, feeding, and signaling? *Antioxid. Redox Signal* **15**, 379–391, doi:10.1089/ars.2010.3678 (2011).

Acknowledgements

We kindly appreciate the support by J.-C. Tardif and R. Margreiter. M. Schneider performed CS analysis. We thank C.L. Hoppel and B. Tandler for helpful comments. H.L. received scholarships from the Canadian NSERC and the Quebec FQRNT. Funding for this work was provided by an NSERC discovery grant to P.U.B. and H.L. (RGPIN 155926 and 402636), K-Regio project MitoFit (EG) and Oroboros Instruments. Contribution to COST Action CA15203 MITOEAGLE. The funders had no role in study design, data collection and analysis, decision to publish, or preparation of the manuscript.

Author Contributions

H.L. performed the experiments, analyzed the data, wrote the manuscript and was involved in funding acquisition. P.U.B. gave suggestions on the discussion section and was responsible for funding acquisition. E.G. designed the study, analyzed the data, wrote and revised the manuscript and was responsible for the resources and project administration.

Additional Information

Competing Interests: E.G. is founder and CEO of OROBOROS INSTRUMENTS, Innsbruck, Austria.

Publisher's note: Springer Nature remains neutral with regard to jurisdictional claims in published maps and institutional affiliations.